PAPER

Check for updates

Separation of vanadium and tungsten from synthetic and spent catalyst leach solutions using an ion-exchange resin†

Jong Hyuk Jeon,[a] Ana Belen Cueva Sola,[ab] Jin-Young Lee,[ab] Janardhan Reddy Koduru [c] and Rajesh Kumar Jyothi [*ab]

Vanadium and tungsten ion adsorption and desorption characteristics and separation conditions were investigated using a simple porous anion-exchange resin. Initially, systematic experimental research was performed using synthetic aqueous vanadium and tungsten solutions. To evaluate the vanadium and tungsten (50–500 mg L^{-1}) isotherm parameters, adsorption was performed at pH 7.0 using 0.5 g of ion-exchange resin at 303 K for 24 h. Well-known adsorption models such as Langmuir, Freundlich, and Temkin were used. Vanadium was desorbed from the resin using HCl and NaOH solutions. In contrast, tungsten was not desorbed by the HCl solution, which enabled the separation of the two ions. The desorption reaction reached equilibrium within 30 min of its start, yielding over 90% desorption. We investigated the adsorption mechanism and resin stability with the aid of spectroscopic and microscopic analysis, as well as adsorption results. The applicability and feasibility of the resin was tested *via* recovery of both metals from real spent catalysts. The applicability and reusability results indicated that the resin can be used for more than five cycles with an efficacy of over 90%.

1. Introduction

Vanadium and tungsten are rare metals. Vanadium is added to steel and special steel to enhance its tensile strength and heat resistance. In addition, it is used as a catalyst in petroleum deoxidation; alcohol and sulphuric acid production; propylene resin synthesis; denitrification; and desulfurization. Tungsten is used widely throughout industry as an alloy, tool steel, electronic device component, chemical raw material, catalyst, inorganic powder, and as a metal itself because of its strong hardness and heat resistance. However, the domestic Korean reserves of these metals are scarce or insufficient and most domestic use heavily depends on imports. Domestic industries are experiencing difficulties with supply and demand because of the instability of the international market and the constant changes in prices. Consequently, there is a big research niche for the different studies on recovering vanadium and tungsten from a variety of waste. In particular, studies have focused on recovery of vanadium and tungsten from waste catalysts, a field

that has increased rapidly in recent years and is expected to expand further in the future. With the introduction of Euro 6 in 2015, the demand for NO$_x$ removal catalysts and the generation of spent catalysts have been increasing significantly. Thus, there is an urgent need for further research.

Metallic elements such as vanadium and tungsten have been recovered from spent catalysts *via* techniques including solvent extraction (liquid–liquid extraction), ion exchange, and precipitation. Luo *et al.* (2003) reported that 86.96% of ammonium metavanadate and 85 to 90 wt% ammonium tungstate were recovered from tungsten alloy scrap using a precipitation technique.[1] The precipitation method is a simple and quick operation in which metal ions precipitate from a solution *via* the addition of a precipitant in the form of an aqueous or non-aqueous solution. However, since various elements are precipitated together in this process, treatment of impurities is difficult. This adversely affects the performance and efficiency of the product, and thus limits application of this technique. With regard to the solvent extraction method, acidic extracting agents such as D2EHPA, PC-88A, and Aliquat 336, and basic extractants including Alamine 336, are the most widely used extracting and separating agents. In this approach, an acidic or basic extracting agent is added to an aqueous solution that contains metal ions. Cueva *et al.* (2020) reported the extraction and enrichment of a vanadium- and tungsten-containing leach liquor obtained from spent SCR catalysts using Aliquat 336. This was followed by stripping at 55 °C with a mixture of NaOH and NaCl. Their research group enriched the solution seven times using

[a]Mineral Resources Division, Korea Institute of Geoscience and Mineral Resources (KIGAM), Daejeon 34132, Korea. E-mail: rkumarphd@kigam.re.kr; Fax: +82-42-868-3421; Tel: +82-42-868-3313

[b]Department of Resources Engineering, Korea University of Science and Technology (UST), Daejeon 34113, Korea

[c]Department of Environmental Engineering, Kwangwoon University, Nowon-gu, Seoul 01897, Korea

† Electronic supplementary information (ESI) available. See DOI: 10.1039/d1ra05253e

a 0.5 mol L^{-1} Aliquat 336 solution. The resulting material was processed further *via* selective precipitation to obtain the title elements.[2,3] Lozano *et al.* (2003) reported vanadium recovery and extraction characteristics obtained when extracting the metal from an aqueous sulphate solution using Primene R81 and Alamine 336.[4] Ahn and Ahn (2008) studied vanadium extraction during solvent extraction of vanadium and titanium using Alamine 336. Although the extraction rate was approximately 40% at pH 1.0, it increased to more than 96% and >99.8% at pH ~2.5 and 4.0, respectively.[5] Gerhardt *et al.* (2001) reported extraction of 99.9% of tungsten using diisododecylamine (DIDA) and separation of tungsten, molybdenum, and rhenium from ore leachate.[6] The separation and recovery of metal ions *via* solvent extraction method is limited in that one must select the extraction agent based on conditions such as the solution pH. Furthermore, separating the suspended materials and precipitates generated during extraction is difficult and requires extensive research.

Alternatively, separation and recovery of metal ions using an ion-exchange resin enables the reversible exchange of ions with the same charge between the ion bearing solution and the ion-exchange resin. Thus, separation can be performed based on the characteristics of the ions and the ion-exchange resin properties.[7–11] This method has recently attracted significant attention, as it can selectively remove metal ions while reducing the solution contamination by impurities. In addition, since they can be regenerated after desorption, ion-exchange resins are economical to use. Furthermore, the adsorption and desorption preparation processes are simple.

After performing a study using ion-exchange resins, Hu *et al.* (2009) reported that 99.5% of vanadium was removed from a molybdate solution *via* adsorption using a strongly basic anion-exchange resin (D296).[12] Ahn *et al.* (2003) reported the preparation of molybdate solution from a solution that contained molybdenum and tungsten.[13] Adsorption experiments performed using chelating resins have demonstrated the possibility of effectively separating molybdenum and tungsten *via* adsorption in the 1.0 to 6.0 pH range.[12,13]

Some papers[14,15] have described comprehensive biosorption investigations and highlighted that biosorption can bridge the gap between laboratory results and industrial applications. They have also demonstrated the importance of the green biosorption approach to applications such as toxic metal removal using the ion-exchange approach.[16] Another study used phosphoryl-functionalised algal-PEI beads and algae biomass to adsorb rare earths and molybdenum.[17,18] The agitation modes involved in mechanical, ultrasonic, and microwave techniques during uranium sorption using amine- and di-thizone-based magnetic chitosan hybrid materials were studied thoroughly.[19] Using a 2-mercapto-benzimidazole derivative of chitosan as a sorbent reagent enabled the sonication effect to improve silver metal recovery.[20] However, the recovery and separation of waste from vanadium and tungsten-containing selective catalytic reduction (SCR) denitrification catalysts *via* ion exchange has been rarely studied. In addition, detailed studies on the ion-exchange resin adsorption and desorption mechanisms of vanadium and tungsten and their related reaction formulas are

insufficient. Therefore, in this study, we investigated the mechanisms by which vanadium and tungsten adsorb and desorb from mixed solutions of SCR denitrification waste catalysts and determined the factors that affect the reaction. The ion-exchange resin used in this study was a porous, strongly basic anion-exchange resin known to be effective in the adsorption of metal ions in solution.

2. Experimental

The synthetic solution was prepared by dissolving ammonium metavanadate (NH_4VO_3, 99% purity), MW 116.98, Samchun Chemicals, Korea) and ammonium tungstate pentahydrate ($5(NH_4)_2O \cdot 12WO_3 \cdot 5H_2O$ (WO_3 content 88 to 90%), MW 3132.52, Kanto Chemicals, Japan) in distilled water to allow the determination of the ion-exchange resin adsorption and desorption characteristics of vanadium and tungsten ions. A 250 mL Pyrex reactor was employed for the batch experiments and the solution acidity was controlled using aqueous HCl and NaOH solutions. The ion-exchange resin used in the adsorption experiments was a porous anion-exchange resin Lewatit Monoplus MP600 (Lanxess, Germany) that uses the Cl$^-$ group as the exchanger (Fig. 1). The physical and chemical properties of this resin are listed in Table 1. Brunauer–Emmett–Teller (BET) surface analysis (Table 1) obtained a surface area of 68.8 m^2 g^{-1}, pore volume of 0.1434 cm^3 g^{-1}, and pore size of 25.928 nm for the as-prepared Lewatit Monoplus MP600 (resin). This indicates that the resin is a mesoporous surface morphology.

In order to evaluate vanadium and tungsten ion adsorption and desorption characteristics using the ion-exchange resin, adsorption equilibrium experiments and adsorption rate experiments were carried out using the synthetic aqueous
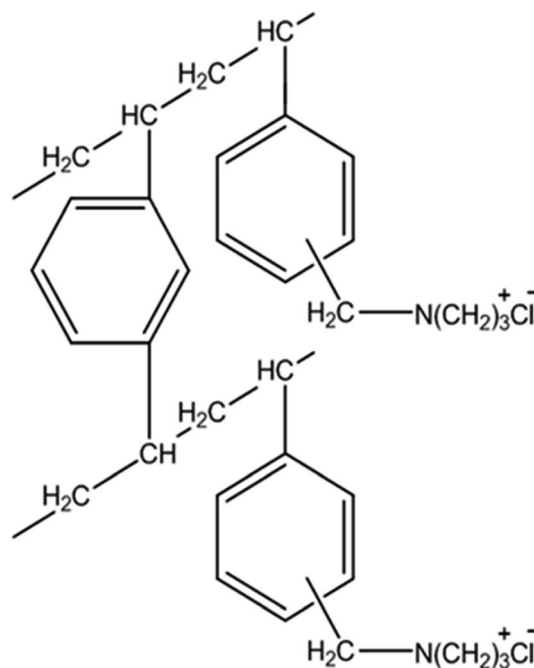

Fig. 1 Structure of Lewatit Monoplus MP600 resin.

Table 1 The physical and chemical characteristics of Lewatit Mono-plus MP600 (resin)

Characteristics of the resin	Remarks
Trade name of the resin	MP 600
Supplier	Lanxess, Germany
Ionic form as shipped	Cl^-
Functional group	Quaternary amine, type II
Matrix	Cross linked polystyrene
Structure	Macroporous
Appearance	Beige, opaque
Uniformity coefficient (max.)	1.1
Mean bead size (mm)	0.6 ($\pm$0.05)
Bulk density ($\pm$5%) (g L^{-1})	630
Density (approx. g mL^{-1})	1.10
Water retention (wt%)	5560
Total capacity (min. eq. L^{-1})	1.1
Volume change (Cl $\rightarrow$ OH) (max. vol%)	12
Stability (at pH-range)	0 to 14
Storability of product (max. year)	2
Storability temperature range (°C)	-20 to $+40$
BET surface area of resin	22.125 m^2 g^{-1}
Single point surface area at P/P_o	21.272 m^2 g^{-1}
Langmuir surface area	32.355 m^2 g^{-1}
Average pore volume	0.1434 cm^3 g^{-1}
Average pore size	25.928 nm

solution of ammonium metavanadate and ammonium tungstate pentahydrate in distilled water. Desorption experiments were performed based on the molar concentrations of HCl and NaOH.

The adsorption equilibrium experiment was carried out as a batch experiment in a shaking incubator. The quantity of ion-exchange resin was fixed and the adsorption rate was tested according to the initial acidity of the solution. An equimolar adsorption isotherm was measured with respect to the metal concentration. The metal adsorption rate was determined by treating 50 mL of the synthetic solution containing 500 mg L^{-1} each of vanadium and tungsten in the 1.0 to 13.0 pH range. This was followed by adding 0.3 g of ion-exchange resin and stirring at 303 K and 200 rpm for 1440 min. In the isothermal adsorption experiment, 0.5 g of resin was added to a solution containing vanadium and tungsten ions in the 50 to 500 mg L^{-1} concentration range. The mixture was stirred at 303 K and 200 rpm for 1440 min.

The adsorption rate tests were performed by adding 0.5 g of ion-exchange resin to 100 mL of a synthetic solution that contained 500 mg L^{-1} each of vanadium and tungsten, stirring for 1 to 1100 min, and collecting samples each hour.

Desorption experiments were performed to evaluate the desorption capabilities of the process as a function of the initial acidity and HCl or NaOH concentration. For the desorption experiment, 0.5 g of ion-exchange resin was added to a synthetic solution that contained 500 mg L^{-1} each of vanadium and tungsten and stirred for 1440 min. After reaching maximum adsorption, the ion-exchange resin was collected, washed with aqueous HCl (2 mol L^{-1}) and NaOH (3 mol L^{-1}) solution, and dried. For the process, the solution was stirred at 200 rpm and 303 K for 1 to 240 min and samples were taken at every hour.

The quantities of vanadium and tungsten ions adsorbed by the ion-exchange resin were determined by measuring the vanadium and tungsten concentrations after the adsorption reaction. We used eqn (1) to determine the volume of the solution and the amount of ion-exchange resin added.

$$q_e = \frac{(C_0 - C_e)V}{W} \tag{1}$$

Here, q_e is the metal adsorption capacity (mg g^{-1}), C_e is the metal concentration (mg L^{-1}) at adsorption equilibrium, V is the total initial volume of the adsorbate solution (L) taken, and W is the dose of adsorbent added (g). The vanadium and tungsten ion concentrations in the solution were measured using ICP-OES (Optima 2000 DV, PerkinElmer Inc.).

3. Results and discussion

3.1 Resin characterization and stability

The SEM (Fig. 2(A)) results show the crystalline porous surface morphology of the resin. Further, the SEM images of resin with metal adsorbed and desorbed indicate that the surface morphology does not change significantly even when highly acidic and basic conditions are used for adsorption and desorption of metal ions. These results show that the resin is a suitable candidate for sustainable adsorption of both metal ions and that the system provides reusability that can reduce process and installation costs. The pore morphology and stability are further confirmed via XRD analysis.

The resin XRD pattern (Fig. 2(B)) include a 2θ peak at 20° that indicates the mesoporous crystalline structure of the resin,[21] which may help provide high adsorption of the target metal ions. Further, the XRD spectra taken after of adsorption at pH 1 and 7 exhibit significant changes in the resin XRD patterns with 2θ peaks at 10° and a broad peak at 20–30°. These may be related to adsorption of metal ions on the resin with a reduction[22,23] or may involve a change in resin texture caused by conversion of amine groups.[24] However, desorption of metals using 2 mol L^{-1} HCl and NaOH significantly influences the resin texture, as observed via the XRD spectrum. Desorption of metal using 2 mol L^{-1} NaOH seems to restore the original texture with small extra peaks at 2θ of 45° and 50° which helps reach the conclusion that there could be a multi-cycle reuse of the resin for the current process. The overall XRD results indicate that the resin is stable and retains its porous texture even after adsorption and desorption of both metal ions under different acidic conditions. Thus, we can restore the original resin structure using 2 mol L^{-1} NaOH (Fig. 2(B)) after desorption of metal ions either in acidic or basic conditions. Further, the FT-IR spectrum (Fig. 2(C)) confirms the resin structure.

In the FT-IR spectrum the broadband in the area of 3100–3500 cm^{-1} is ascribed to –N–H vibrations and the peak at 1490 cm^{-1} indicates $-N^+(CH_2)_3$ moieties.[25] Moreover, the sharp peak near 2900 cm^{-1} is ascribed the presence of the –C–C– stretching vibration in the resin. The peaks at 1200–1500 cm^{-1} are ascribed to the –C–N– bond frequency. The sharp peak at 1600 cm^{-1} indicates –C=C– stretching vibrations. The peaks that appear in the area of 1000 to 800 cm^{-1} are ascribed to benzene ring –C=C– bands. After adsorption in acidic
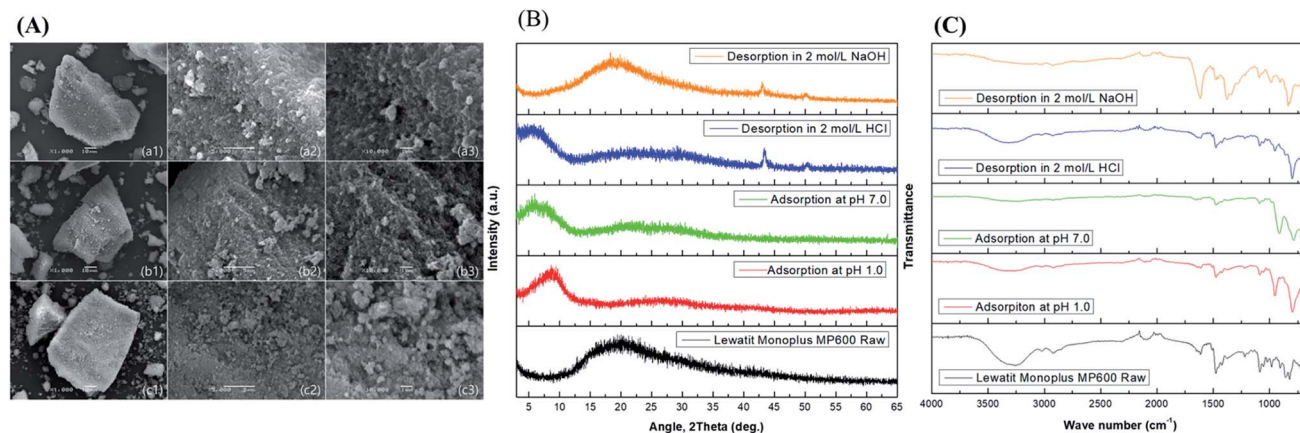
Fig. 2 (A) SEM images of the source resin along with metal ions adsorption and desorption conditions ((a1–a3) SEM pictures are before adsorption (raw resin), (b1–b3) SEM pictures are after adsorption and (c1–c3) SEM pictures are after desorption); (B) XRD pattern of the source resin along with title metal ions adsorption and desorption conditions; (C) FT-IR pattern of the source resin along with title metal ions adsorption and desorption conditions.

conditions or at pH 7.0, the positions of the peaks at 1200–1500 cm^{-1}, 1600 cm^{-1}, and in the area of 1000 to 800 cm^{-1} are altered. This indicates the loading of metal ions on the resin. These results confirm that metal ions are adsorbed predominantly *via* π–π bonding electrons rather than other functions on the surface of the resin. However, the functional groups are relocated to their original positions after desorption. The results are almost the same after desorption using 2 mol L^{-1} HCl and 2 mol L^{-1} NaOH. These results confirm the stability of the resin and that it can be reused multiple times.

3.2 Effect of the initial adsorption process pH

The initial pH of the solution has an important effect on the adsorption performance of the adsorbent because it affects the form of the metal ion in the solution or how the adsorption process performs in a batch reactor. It is possible to optimise the performance of the adsorption process by optimising the soluble pH range of the ion-exchange resin. Moreover, the binding form of the metal ion depends on the acidity of the solution and also plays a large role in the adsorption reaction. It is difficult to control the solution acidity in a batch reactor, as the solution pH changes during the adsorption reaction. In order to investigate the effect of the initial solution acidity on adsorption performance, an experiment was performed using 0.3 g of ion-exchange resin in 50 mL of solution using initial pH values in the 1.0 to 13.0 range. The initial metal (V or W) concentrations were 500 mg L^{-1}. Aqueous HCl and aqueous NaOH were used to adjust the solution pH.

The vanadium and tungsten adsorption behaviours vary with the initial acidity of the solution (Fig. 3(A)). Vanadium almost
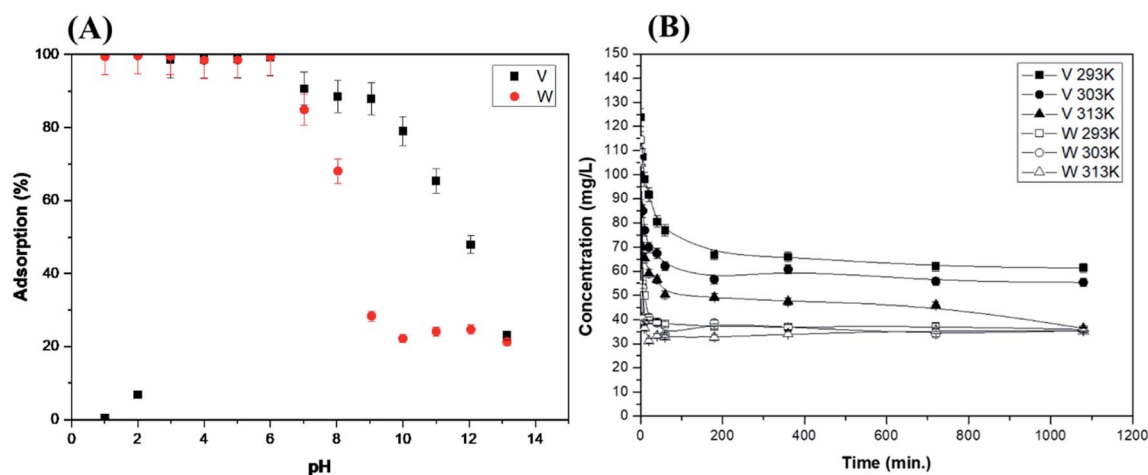

Fig. 3 (A) Effect of initial pH on the adsorption of vanadium and tungsten on MP600, (B) effect of temperature on the adsorption of vanadium and tungsten (experimental conditions for pH effect: initial pH range is 1 to 14, temperature at 303 K, initial concentration of the metals are $V = 500$ mg L^{-1} and $W = 500$ mg L^{-1}, agitation rate is 200 rpm, volume is 100 mL, resin dose is 0.5 g, reaction time is 1440 min and experimental conditions for kinetic study is: temperature ranging 293 to 313 K, initial concentration of the metals are $V = 120$ mg L^{-1} and $W = 120$ mg L^{-1}, agitation rate is 200 rpm, volume is 100 mL, resin dose is 0.1 g).

does not adsorb at pH 1.0 and 2.0. The adsorption rates of both ions decrease at pH ≥ 6.0, in addition to decreasing drastically in a strongly basic environment. Vanadium is present in the cationic form at pH 1.5, whereas it exists in the anionic form at pH > 1.5. Stable anionic vanadium adsorbs to anion-exchange resins quite easily in the 2.0–10.0 pH range. Tungsten shows a high adsorption rate in the acidic 1.0–6.0 pH range, but the adsorption rate tends to decrease at pH ≥ 9.0. The binding form of tungsten ions is obtained from the Eh-pH diagram as a function of solution acidity. The higher the basicity of the solution, the higher the ratio of WO_4^{2-}. Various types of poly-oxides appear if the acidity is increased by adding acid (pH decrease). Polyoxometalate anions appear as $[W_{10}O_{32}]^{4-}$ at pH 1.0–2.0, $[H_2W_{12}O_{40}]^{6-}$ in the 2.0–4.0 pH range, and $[W_7O_{24}]^{6-}$ and $[H_2W_{12}O_{42}]^{10-}$ in the 5.0–9.0 pH range. They precipitate as $WO_3 \cdot 2H_2O$ under strong acidic conditions (pH < 1.0). There-fore, tungsten exhibits optimum adsorption performance when it is present in the form of $[H_2W_{12}O_{40}]^{6-}$ or $[W_7O_{24}]^{6-}$.

3.3 Effect of temperature

The reaction temperature affects the reaction rate and the maximum extent of adsorption. The vanadium reaction rate and the maximum adsorption increase with the temperature according to the experiments performed at 293, 303, and 313 K (Fig. 3(B)). However, these increases are small. This suggests that increases in the activation energy of the adsorption reaction between tungsten and the ion-exchange resin do not affect the adsorption process. This phenomenon is demonstrated further using thermodynamic studies in Section 3.6.

3.4 Adsorption isotherms

The Langmuir, Freundlich, and Temkin adsorption isotherm models (Table 2) can be used to identify the adsorption mechanism *via* fitting the absorbate behaviour in equilibrium to one of the different models. The Langmuir adsorption isotherm assumes that the adsorbate forms a monolayer on the surface of the adsorbent. Here, b and q are Langmuir constants related to the adsorption rate and capacity, respectively.

The Freundlich adsorption isotherm assumes that the adsorbent surface adsorbs to a multi-molecular layer considering the interaction between adsorbed metal ions with non-uniform surface energies. In this equation, K_F, and n are constants that represent the suitability of the adsorption process. K_F is the adsorption capacity, and $1/n$ is the slope. Respectively, they represent the adsorption strength and non-uniformity. The slope approaches zero as the non-uniformity increases.

The Temkin isotherm assumes a linear reduction in the heat of adsorption rather than a logarithmic drop, but disregards extremely high and low concentrations. It also implies that the bounding energy is distributed uniformly up to a certain maximum bonding energy. Here, K_o is the Temkin isotherm equilibrium constant (L g^{-1}), T is the absolute temperature (K), R is the gas constant (8.314 J mol^{-1} K^{-1}), and $RT/\Delta Q$ is the Temkin constant (J mol^{-1}). The Langmuir, Freundlich, and Temkin adsorption isotherms are shown in Fig. S1† and the constants related to each adsorption isotherm are listed in Table 2. The suitability of the vanadium and tungsten data to isotherm model was evaluated using the correlation coefficient (R^2) and statistical error, Pearson's correlation coefficient (r).

The Langmuir, Freundlich, and Temkin adsorption isotherm correlation coefficients (R^2) for vanadium are 0.974, 0.644, and 0.770 respectively. This indicates that the Langmuir adsorption isotherm is the most suitable for explaining the vanadium ion isothermal adsorption experiment results. Further, the superior suitability of the Langmuir isotherm is confirmed *via* Pearson's correlation coefficient ($r = 0.993$), which is closer to 1 than those produced by the other isotherms in the case of vanadium. The Langmuir, Freundlich, and Temkin isothermal adsorption correlations and Pearson coefficients for tungsten all explain tungsten adsorption onto the resin well. However, the Freundlich and Temkin isotherms are confirmed to be most suitable based on their Pearson's correlation coefficients ($r = 0.977$ and 0.988 for the Freundlich and Temkin isotherms, respectively). The coefficients are close to 1 in the case of tungsten. Adsorption of vanadium ions to ion-exchange resins follows typical monolayer ion-exchange adsorption, whereas adsorption of tungsten ions is similar to a multimolecular adsorption by interacting ions by the poly-oxo-metalation of tungsten ions. According to the Eh-pH diagram, the proportion of WO_4^{2-} in the solution increases as the basicity of the solution increases. The same concept applies to $[W_{10}O_{32}]^{4-}$ at pH 1 to 2,

Table 2 Isotherm parameters of vanadium and tungsten (50 to 500 mg L^{-1}) adsorption process[a]

	Langmuir				Freundlich				Temkin			
	$\dfrac{C_e}{q_e} = \dfrac{C_e}{q} + \dfrac{1}{bq}$				$\log q_e = \log K_F + \dfrac{1}{n}\log C_e$				$q_e = \dfrac{RT}{\Delta Q}\ln K_o C_e$			
	q (mg g^{-1})	b (L mg^{-1})	R^2	Pearson's correlation coefficient, r	K_F ((mg g^{-1}) (L mg^{-1})$^{1/n}$)	$1/n$	R^2	Pearson's correlation coefficient, r	ΔQ (J mol^{-1})	K_o (L mg^{-1})	R^2	Pearson's correlation coefficient, r
V	75.301	1.564	0.974	0.993	53.469	0.078	0.644	0.845	3.337×10^2	3.786×10^7	0.770	0.877
W	69.160	7.692	0.933	0.982	52.869	0.101	0.946	0.977	8.149×10^7	2.402×10^9	0.976	0.988

[a] Experimental conditions: initial pH is 7.0 using 0.5 g of ion exchange resin, temperature at 303 K and stirring is 200 rpm, reaction time is 1440 min, volume of the aqueous solution is 100 mL.

$[H_2W_{12}O_{40}]^{6-}$ at pH 2 to 4, $[W_7O_{24}]^{6-}$ and $[H_2W_{12}O_{42}]^{10-}$ at pH 5 to 9, and $WO_3 \cdot 2H_2O$ in strongly acidic solutions. Adsorption of the polyoxometallate ion affects the form in which tungsten adsorption occurs on the ion-exchange resin.

The suitability of the Freundlich adsorption isotherm is judged by the distribution of the $1/n$ value, as suggested by Fukukawa. Effective adsorption is possible when the $1/n$ value is in the range of 0.1 to 0.5. In this experiment, the $1/n$ value of vanadium is not suitable (0.078) and that of tungsten is 0.1007. This indicates that the adsorption of tungsten is explained well by the Freundlich adsorption isotherm.[23,26–31]

3.5 Kinetic studies of the adsorption process

Adsorption kinetics provides quantitative analysis of the vanadium and tungsten ion adsorption rates observed using ion-exchange resins. Pseudo-first-order (PFO) and pseudo-second-order (PSO) models were used. The pseudo-first-order (eqn (2)) adsorption model can be represented as follows.

$$\ln(q_e - q_t) = \ln q_e - k_1 t \tag{2}$$

where k_1 is the first-order rate constant (min^{-1}); q_e and q_t are the quantities of adsorbed metal (mg g^{-1}) at equilibrium and at a determined time t (min), respectively. The values obtained by applying eqn (2) to adsorption rate experiment data are shown in Fig. S2.† PFO kinetic parameters are listed in Table 3 to enable understanding of the kinetic process.

A similar quadratic reaction rate model was proposed by Ho and Mckay based on the adsorption equilibrium capability[31]

$$\frac{t}{q_t} = \frac{1}{k_2 q_e^2} + \frac{1}{q_e} t \tag{3}$$

where k_2 is the second-order rate constant $(\text{g mg}^{-1} \text{min}^{-1})$, q_e, and q_t are the amounts of metal adsorbed at equilibrium (mg g^{-1}), and at a determined time t (min).

The k_2, q_e, and R^2 values can be obtained from the slope and intercept of the above linear equation, where h $(\text{mg g}^{-1} \text{min}^{-1})$ is the initial rate of adsorption.

$$h = k_2 q_e^2 \tag{4}$$

The adsorption rate experiment results are shown in Fig. S2.† PSO kinetic parameter values are listed in Table 3 to enable understanding of the kinetic process.

The equilibrium adsorption $q_{e,cal}$ obtained from the similar PFO and PSO kinetic models and the equilibrium adsorption $q_{e,exp}$ obtained from the actual experiment are compared to the calculated values and $q_{e,cal}$ from the proposed models. The PSO model is found to be most suitable for representing the experimental results (Table 3). The R^2 values indicate that the PSO model responds better to the experimental results as well.

3.6 Thermodynamic studies of the adsorption process

For a better understanding of the vanadium and tungsten adsorption processes that occur using a Lewatit Monoplus MP600, various thermodynamic parameters such as the Gibbs free energy, enthalpy, and entropy were derived using kinetic adsorption parameters measured at various temperatures (293, 303, and 313 K). These thermodynamic parameters provide deep insight into the chemical interactions between the resin and the title elements.

$$\Delta G = -RT \ln K_e \tag{5}$$

$$\Delta G = \Delta H - T\Delta S \tag{6}$$

Upon combining eqn (5) and (6),

$$\ln K_e = \frac{-\Delta H}{RT} + \frac{\Delta S}{R} \tag{7}$$

where, R, the universal gas constant, equals 8.314 J mol^{-1} K^{-1}. K_e is the thermodynamic equilibrium constant and ΔG, ΔH, and ΔS are the Gibbs free energy change, enthalpy change and entropy change, respectively, during the adsorption process.

The slope and intercept of the $\ln K_e$ vs. $1000/T$ plot (Fig. S3†), which is based on the Van't Hoff relation (eqn (5)), correspond to the enthalpy and entropy, respectively. Table 4 shows the enthalpies, entropies, and Gibbs free energies associated with vanadium and tungsten adsorption. The enthalpy has a substantial positive value in the case of vanadium adsorption but a modest negative value in the case of tungsten adsorption. This indicates that the vanadium reaction is endothermic and leads to the realization that even a small temperature increase

Table 3 Kinetic parameters of vanadium and tungsten (500 mg L^{-1}) adsorption at pH 7.0 using 0.5 g of ion exchange resin and stirring at 200 rpm and different temperature[a]

| Metal | Temperature, K | Pseudo 1st order model | | | Pseudo 2nd order model | | | | Experimental, |
		k_1, min^{-1}	$q_{e,cal}$, mg g^{-1}	R^2	k_2, g mg^{-1} min^{-1}	$q_{e,cal}$, mg g^{-1}	h, mg g^{-1} min^{-1}	R^2	$q_{e,exp}$, mg g^{-1}
Vanadium	293	5.97×10^{-3}	33.418	0.922	8.06×10^{-4}	63.412	3.244	0.999	62.460
	303	3.74×10^{-3}	22.365	0.454	1.31×10^{-3}	67.340	5.953	0.999	68.060
	313	4.45×10^{-3}	23.573	0.731	1.47×10^{-3}	78.003	8.959	0.999	77.890
Tungsten	293	4.16×10^{-3}	11.559	0.453	5.54×10^{-3}	78.247	33.887	0.999	78.510
	303	5.44×10^{-3}	15.678	0.737	5.88×10^{-3}	74.906	33.014	0.999	76.250
	313	1.57×10^{-3}	7.162	0.102	-7.28×10^{-3}	69.396	−35.075	0.999	73.470

[a] Experimental conditions: initial pH is 7.0 using 0.1 g of ion exchange resin, temperature varied from 293 to 303 K, stirring is 200 rpm, volume of the aqueous solution is 100 mL, concentration of the metals in feed solution is 120 mg L^{-1} of vanadium (or) tungsten.

Table 4 Thermodynamic results for adsorption of tungsten and vanadium[32–34][a]

Thermodynamic parameter	Name of the metal	
	Vanadium	Tungsten
ΔH, kJ mol^{-1}	19.39	−1.78
ΔS, J K^{-1} mol^{-1}	156.23	101.21
ΔG, kJ mol^{-1} at 298 K	−26.39	−31.40
ΔG, kJ mol^{-1} at 303 K	−27.95	−32.45
ΔG, kJ mol^{-1} at 313 K	−29.51	−33.45

[a] Experimental conditions: initial pH is 7.0 using 0.1 g of ion exchange resin, temperature varied from 293 to 303 K, stirring is 200 rpm, volume of the aqueous solution is 100 mL, concentration of the metals in feed solution is 120 mg L^{-1} of vanadium (or) tungsten.

can increase the quantity of vanadium adsorbed on the resin. Tungsten adsorption, on the other hand, is somewhat exothermic. As shown in Fig. S3,† minor variations in the adsorption temperature have negligible influence on the adsorption process. The positive entropies noted in both cases show an increase in the randomness of the system in concordance to the second law of thermodynamics, which indicates that systems tend to increase their randomness spontaneously. These changes in entropy might occur due to structural changes happening between the metals and the resin during the adsorption process. Finally, the negative Gibbs free energy indicates thermodynamically favourable, spontaneous vanadium and tungsten adsorption processes.[32–34]

3.7 Adsorption-based metal removal mechanisms

The metal removal process was examined for feasibility based on spectroscopic and microscopic examinations such as SEM,

FT-IR, XRD, as well as batch adsorption studies, such as pH studies; kinetics; isotherms; and thermodynamic studies. The study findings demonstrate that metal ions are adsorbed mostly via π–π bonding electrons, rather than other functions on the resin's surface. The pH-effect data show that surface charges and aqueous solution acidity dominate adsorption. Furthermore, the kinetic and isotherm data indicate that monolayer adsorption occurs via surface complexation for both metals. Finally, differences in the adsorption mechanisms of the two metals are described well using thermodynamic studies. Vanadium interactions with resin are endothermic, whereas tungsten interactions are exothermic. The overall results suggest that the removal of metal ions via surface complexation occurs via π–π bonding electrons.

3.8 Desorption studies

Desorption experiments were performed using aqueous HCl and NaOH solutions from 1.0 to 3.0 mol L^{-1} and desorption rates for various desorbing solution types and concentrations were compared. The results are shown in Fig. 4. Increasing the desorption solution concentration increases the desorption rate. In the aqueous HCl solution, the rate of vanadium desorption from MP600 is maximised at 2 mol L^{-1}. Vanadium is desorbed in the aqueous HCl solution, but tungsten is almost impossible to desorb. In contrast, both ions desorb in an aqueous NaOH solution. The adsorption characteristics depend on the initial pH of the solution of the two ions. Vanadium adsorption decreases significantly at a strongly acidic pH of 1.0 and a strongly basic pH of 13.0, whereas tungsten rarely adsorbs under the strongly basic condition of pH 13.0. Separation of vanadium and tungsten is achieved using the contrasting desorption characteristics of the two ions.
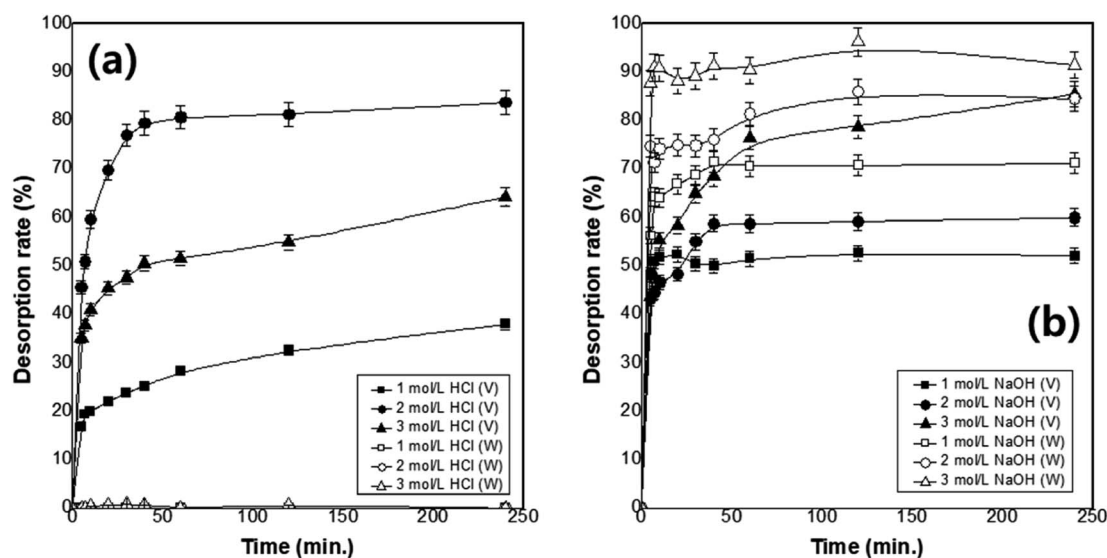

Fig. 4 The desorption rate of vanadium and tungsten for concentrations of desorbing solution (a) HCl (b) NaOH (experimental conditions: aqueous solution ranging from 1.0 to 3.0 mol L^{-1} of HCl and NaOH solutions, temperature at 303 K, agitation rate is 200 rpm, volume is 100 mL, resin dose is 0.5 g).
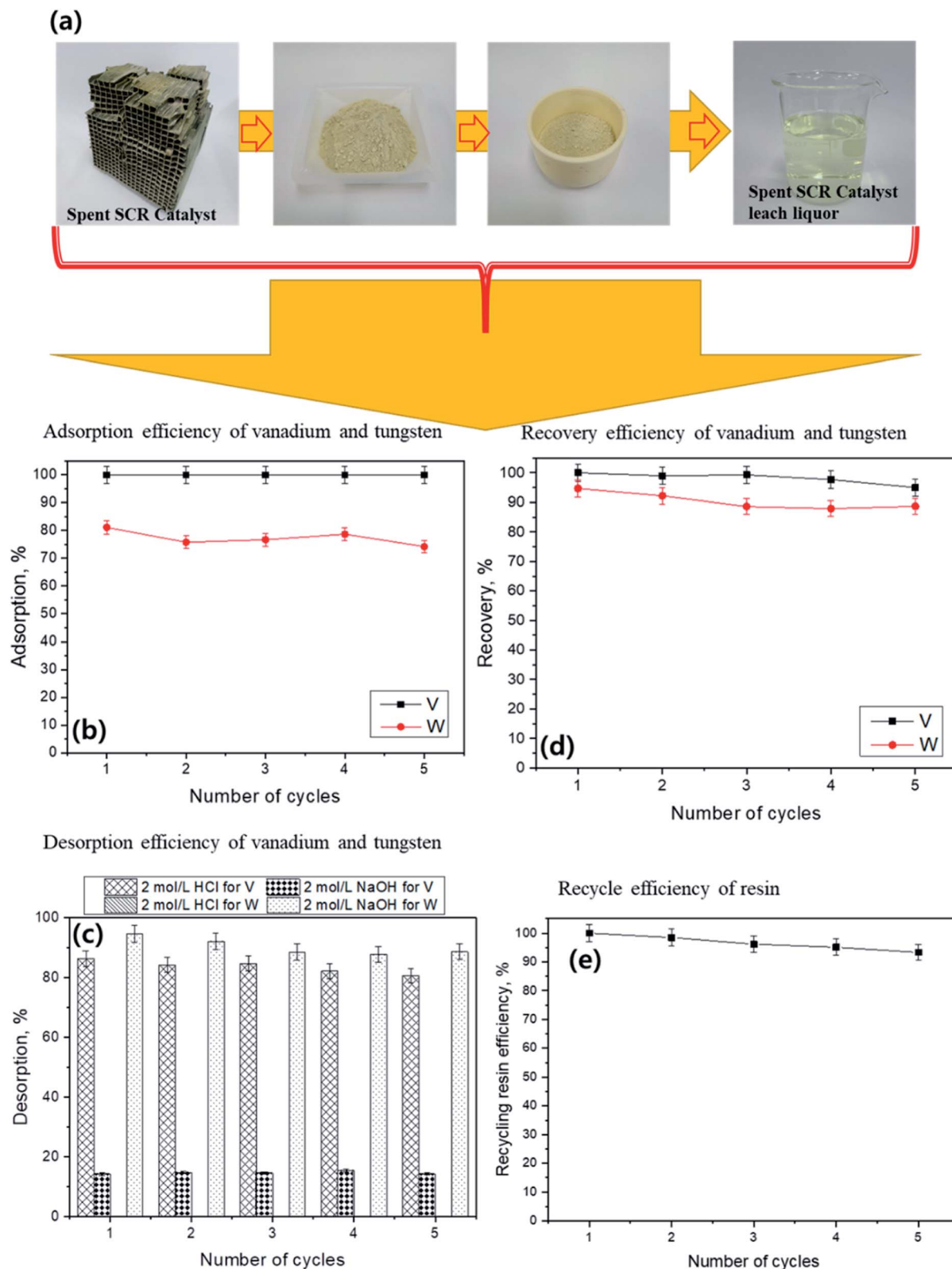
Fig. 5 Application and recycling capacity of the resin (a) represents the total proposed flowsheet of the spent SCR catalysts processing, (b) represents the adsorption of the title metals tested for five cycles, (c) represents the desorption of the title metals tested for five cycles, (d) represents the overall recovery of the title metals tested for five cycles, (e) represents the recycling capacity of the resin for five cycles (experimental conditions for adsorption or desorption: temperature at 303 K, initial concentration of the metals are $V = 100$ mg L^{-1} and $W = 1000$ mg L^{-1}, agitation rate is 200 rpm, volume is 100 mL, resin dose is 0.5 g, reaction time is 1440 min).

Table 5 Comparison of the present developed method with earlier reported literature on vanadium (or) tungsten adsorption studies

Name of the resin (or) adsorbent (or) sorbent	Name of the Metal (s)	Remarks	Reference
Amidoxime resin	Ga, V, Al	Vanadium was maximum adsorbed 26.32 mg g; at 50 °C temperature with 12 mol L^{-1} of NaOH solution was able to eluted 50% of vanadium	35
Poly(styrene-divinylbenzene) (D860) resin and cross-linked acrylic acid (D314) resin	V, Al, Fe, P	Selective extraction of vanadium from 2000 mg L^{-1} of feed, eluted the 5505 mg L^{-1} after eight cycles of process with 30 mol L^{-1} of H_2SO_4 at 20 min time was reported	36
Fabricated resin made with D314 ($N(CH_3)_2$ functional groups and cross-linked acrylate structure) and carbon nanotubes (CNTs) or activated carbon (AC)	V, Al, Fe, P, Si	D314 with activated carbon proved better ion selectivity	37
Herein HZrO@D201, an adsorbent with decoration of nanosized hydrous zirconium oxide (HZrO) on anion exchange resin D201	V, Cl^-, NO_3^-, SO_4^{2-}, PO_4^{3-}	V(v) was adsorbed maximum 118.1 mg g^{-1} at pH range 3 to 9. This study was performed for vanadium polluted ground water treatment	38
Resin 201*7	V, NH_4^+, Si, Al, Fe, Ca, Mg, K, Na	99% of vanadium from 106 mg L^{-1} of feed solution was adsorbed with 1.6 g L^{-1} of resin at pH 6 to 8, temperature, 40 °C adsorption time requires 20 min (other associated elements were adsorbed less than 10%)	39
Anion exchange resins (D201, D301, D314) and cation exchange resin (D860) were fabricated with activated carbon (AC)	V	D860/AC fabricated resin shown the highest adsorption capacity for V(v) at pH 2.0. Whereas other electrode i.e. D314/AC is the optimum due to worthy selective properties, compared with other electrodes	40
The macro-porous resin D301 (analog to Amberlite IRA-9)	W, Mo	The resin D301 showed good selectivity in between title metals such as W and Mo	41 and 42
The macro polyhydroxy chelating resin D403 (resembling Amberlite IRC-743)	W, Mo	W Adsorption was fits the Freundlich model, where as other metal Mo adsorption was fit Henry model. The reaction was endothermic	43
Lewatit Monoplus MP600	V, W	The developed methodology was applied to test real sample such as spent SCR catalyst. The results of applicability and res-usability studies concluded that the resin can be used for more than five cycles without losing its adsorption and re-useable efficacy more than 90%	Present method

3.9 Application of the developed method and resin recycling

To understand its applicability, feasibility, and reusability, the developed ion exchange methodology was applied to a real spent SCR catalyst leach liquor solution. The solution contained 155 mg L^{-1} of vanadium and 1697 mg L^{-1} of tungsten. The resin dosage was 0.5 g for each 100 mL of spent SCR catalyst leach liquor and the reaction proceeded for 24 h. The vanadium and tungsten adsorption, desorption, and recovery efficiencies are presented in Fig. 5. A schematic representation of spent SCR catalyst sample preparation is shown in Fig. 5(A). Fig. 5(B)

shows that 100% of the vanadium is removed from the spent SCR catalyst leach solutions in all studied cycles, whereas >80% removal of tungsten is achieved. Further, the resin desorption ability of each metal is studied in Fig. 5(C) using five cycles of 2 mol L^{-1} HCl and NaOH. More than 95% of vanadium and 0% of tungsten are desorbed by HCl on each cycle. When NaOH is used as the desorbing agent, more than 95% of tungsten and less than 15.4% of vanadium desorb during each cycle. This results indicate that the selective desorption of vanadium and tungsten can be achieved using 2 mol L^{-1} of HCl and 2 mol L^{-1}

of NaOH, respectively. This indicates the potential feasibility of real separation and recovery of the two metals. In addition, more than 95% recovery of vanadium from spent SCR catalyst is achieved for each cycle (up to five cycles) of resin reuse (Fig. 5(D)). In contrast, tungsten recovery exceeds 90% for the first two cycles and decreases to approximately 88.5% during later cycles. Further, the recycled resin adsorption efficiency exceeds 96% for first 3 cycles for both metals. It then decreases to 95% and 93.3% in the 4th and 5th cycles, respectively (Fig. 5(E)). The overall results indicate that the resin might be used for more than five cycles of vanadium and tungsten adsorption with a recovery of more than 90% from real leach liquor, those experiments prove the feasibility and cost-effectiveness for sustainable application.

The developed adsorption and desorption methodology is compared to earlier reports on vanadium and tungsten adsorption in Table 5.[35–43] The present metal removal and separation method is comparable to previously reported methods.

4. Conclusions

The Langmuir, Freundlich, and Temkin adsorption isotherm fitting results showed that both vanadium and tungsten adsorption fit the Langmuir adsorption model. Tungsten adsorption was also compatible with the Freundlich and Temkin adsorption isotherms which is similar to a polymolecular adsorption *via* polyoxometallation, in which the interaction and bonding between ions changes with the acidity of the solution. The PFO and PSO reaction kinetics showed that both of the ion-exchange resins could be simulated well *via* PSO reaction rate models. The theoretical and experimental values were in agreement with each other. Vanadium was desorbed in both acidic and basic solutions, whereas tungsten was desorbed only in the basic solution. Therefore, it was possible to separate the two ions completely using the difference between the vanadium and tungsten desorption characteristics. The desorption ratio also increased with the desorption solution concentration. Equilibrium was reached within 30 min of the start of the desorption reaction, and ≥90% recovery was confirmed. Batch studies confirmed that adsorption occurred *via* physisorption. This was confirmed further *via* instrumental characterization. SEM, XRD, and FT-IR data collected before and after adsorption showed that adsorption of both metal ions occurred *via* interaction of the π–π electrons in the resin and constituted physisorption. Further, these results confirmed the stability of the resin even under high acidic and alkaline conditions. In addition, the applicability and reusability study results showed that the resin can be used for more than five cycles without losing its adsorption capabilities and retains efficacy of more than 90% during reuse.

Author contributions

Dr Jong Hyuk Jeon performed all of the experiments and wrote the manuscript. Ms Ana Belen Cueva Sola calculated the thermodynamic data and did the formal analysis. Prof. Janardhan Reddy Koduru edited the manuscript and checked the data. Prof. Jin-Young Lee and Prof. Rajesh Kumar Jyothi supervised the experiments and performed formal analysis and editing of the manuscript.

Conflicts of interest

The authors declare that they have no known competing financial interests or personal relationships that could appear to influence the work reported in this paper.

Acknowledgements

Notes and references

1 L. Luo, T. Miyazaki, A. Shibayama, W. Yen and T. Fujita, *Miner. Eng.*, 2003, **16**, 665–670.

2 A. B. Cueva Sola, P. K. Parhi, J. Y. Lee, H. N. Kang and R. K. Jyothi, *RSC Adv.*, 2020, **10**, 19736–19746.

3 A. B. Cueva Sola, J. Jeon, J. Y. Lee, P. K. Parhi and R. K. Jyothi, *J. Korean Inst. Resour. Recycl.*, 2020, **29**, 55–61.

4 L. J. Lozano and C. Godínez, *Miner. Eng.*, 2003, **16**, 291–294.

5 J. G. Ahn and J. W. Ahn, *J. Korean Inst. Met. Mater.*, 2008, **46**, 823–829.

6 N. Iatsenko Gerhardt, A. A. Palant and S. R. Dungan, *Hydrometallurgy*, 2000, **55**, 1–15.

7 N. V. Chukanov, S. M. Aksenov, I. V. Pekov, N. A. Chervonnaya, D. A. Varlamov, V. N. Ermolaeva and S. N. Britvin, *Microporous Mesoporous Mater.*, 2021, **312**, 110776.

8 A. Jankowska, A. Chłopek, A. Kowalczyk, M. Rutkowska, W. Mozgawa, M. Michalik, S. Liu and L. Chmielarz, *Microporous Mesoporous Mater.*, 2021, **315**, 110920.

9 C. Hernandez-Tamargo, B. Kwakye-Awuah, A. J. O'Malley and N. H. de Leeuw, *Microporous Mesoporous Mater.*, 2021, **315**, 110903.

10 T. Ikeda, Y. Yoshida, N. Nakazawa, S. Inagaki and Y. Kubota, *Microporous Mesoporous Mater.*, 2020, **302**, 110197.

11 A. A. C. Reule, V. Prasad and N. Semagina, *Microporous Mesoporous Mater.*, 2018, **263**, 220–230.

12 J. Hu, X. Wang, L. Xiao, S. Song and B. Zhang, *Hydrometallurgy*, 2009, **95**, 203–206.

13 J.-H. Ahn, B.-R. Kim and Y. G. Seo, *J. Korean Ind. Eng. Chem.*, 2000, **11**, 232–238.

14 A. M. Elgarahy, K. Z. Elwakeel, S. H. Mohammad and G. A. Elshoubaky, *Clean. Eng. Technol.*, 2021, **4**, 100209.

15 A. M. Elgarahy, K. Z. Elwakeel, A. Akhdhar and M. F. Hamza, *Nanotechnol. Environ. Eng.*, 2021, **6**, 1–24.

16 H. G. El-Shorbagy, S. M. El-Kousy, K. Z. Elwakeel and M. A. A. El-Ghaffar, *J. Ind. Eng. Chem.*, 2021, **100**, 410–421.

17 Y. Wei, K. A. M. Salih, K. Rabie, K. Z. Elwakeel, Y. E. Zayed, M. F. Hamza and E. Guibal, *Chem. Eng. J.*, 2021, **412**, 127399.

18 C. He, K. A. M. Salih, Y. Wei, H. Mira, A. A.-H. Abdel-Rahman, K. Z. Elwakeel, M. F. Hamza and E. Guibal, *Metals*, 2021, **11**, 294.

19 K. Z. Elwakeel, M. F. Hamza and E. Guibal, *Chem. Eng. J.*, 2021, **411**, 128553.

20 K. Z. Elwakeel, A. S. Al-Bogami and E. Guibal, *Chem. Eng. J.*, 2021, **403**, 126265.

21 N. Q. Yin, P. Wu, T. H. Yang and M. Wang, *RSC Adv.*, 2017, **7**, 9123–9129.

22 A. B. Khatibani, M. Abbasi and S. M. Rozati, *Acta Phys. Pol., A*, 2016, **129**, 1245–1251.

23 S. V. Pol, V. G. Pol, V. G. Kessler and A. Gedanken, *New J. Chem.*, 2006, **30**, 370–376.

24 A. Wołowicz and Z. Hubicki, *Microporous Mesoporous Mater.*, 2016, **224**, 400–414.

25 J. Ma, C. Wang and H. He, *Appl. Catal., B*, 2016, **184**, 28–34.

26 P. Cyganowski, I. Polowczyk, D. V. Morales, B. F. Urbano, B. L. Rivas, M. Bryjak and N. Kabay, *Polym. Bull.*, 2018, **75**, 729–746.

27 B. J. Smith and V. A. Patrick, *Aust. J. Chem.*, 2002, **55**, 281–286.

28 K. R. Hall, L. C. Eagleton, A. Acrivos and T. Vermeulen, *Ind. Eng. Chem. Fundam.*, 1966, **5**, 212–223.

29 J.-J. Lee, J.-H. Cho and H.-T. Kim, *Clean Technol.*, 2011, **17**, 346–352.

30 P. Sampranpiboon and P. Charnkeitkong, *Int. J. Energy Environ.*, 2010, **4**, 88–98.

31 Y. S. Ho and G. McKay, *Process Biochem.*, 1999, **34**, 451–465.

32 J. C. Callura, K. M. Perkins, J. P. Baltrus, N. R. Washburn, D. A. Dzombak and A. K. Karamalidis, *J. Colloid Interface Sci.*, 2019, **557**, 465–477.

33 É. C. Lima, M. H. Dehghani, A. Guleria, F. Sher, R. R. Karri, G. L. Dotto and H. N. Tran, in *Green Technologies for the Defluoridation of Water*, Elsevier, 2021, pp. 41–88.

34 L. P. Lingamdinne, Y. Y. Chang, J. K. Yang, J. Singh, E. H. Choi, M. Shiratani, J. R. Koduru and P. Attri, *Chem. Eng. J.*, 2017, **307**, 74–84.

35 Q. Zheng, C. He, J. Meng, T. Fujita, C. Zheng, W. Dai and Y. Wei, *Solvent Extr. Ion Exch.*, 2021, **39**, 373–398.

36 S. Bao, B. Chen, Y. Zhang and Y. Cui, *Chem. Eng. Res. Des.*, 2020, **163**, 107–114.

37 Q. Chen, S. Bao and Y. Zhang, *Chem. Eng. Technol.*, 2020, **43**, 1588–1595.

38 M. Li, B. Zhang, S. Zou, Q. Liu and M. Yang, *J. Hazard. Mater.*, 2020, **384**, 121386.

39 X. Zhu, W. Li and C. Zhang, *Environ. Res.*, 2020, **180**, 108865.

40 Y. Cui, S. Bao, Y. Zhang and J. Duan, *Chemosphere*, 2018, **212**, 34–40.

41 J. Zhang, X. Liu, X. Chen, J. Li and Z. Zhao, *Hydrometallurgy*, 2014, **144–145**, 77–85.

42 Z. Zhao, J. Zhang, X. Chen, X. Liu, J. Li and W. Zhang, *Hydrometallurgy*, 2013, **140**, 120–127.

43 X. Zhu, G. Huo, J. Ni and Q. Song, *J. Cent. South Univ.*, 2016, **23**, 1052–1057.